Hindawi Publishing Corporation
International Journal of Corrosion
Volume 2012, Article ID 146486, 9 pages
doi:10.1155/2012/146486

Research Article

Corrosion Behavior of Fe40Al Alloy with Additions of Ti, Ag, and Cr in Molten KCl + $ZnCl_2$

R. Ademar,[1] J. G. Gonzalez-Rodriguez,[1] J. Uruchurtu,[1] J. Porcayo-Calderon,[2] V. M. Salinas-Bravo,[2] G. Dominguez-Patiño,[3] and A. Bedolla-Jacuinde[4]

[1] *U.A.E.M.-C.I.I.C.A.P. Av. Universidad 1001, Col. Chamilpa, 62500-Cuernavaca, Mor., Mexico*
[2] *I.I.E., Gerencia de Procesos Termico, Av. Reforma 120, Temixco, Mor., Mexico*
[3] *U.A.E.M.-Facultad de Biología, Av. Universidad 1001, Col. Chamilpa, 62500-Cuernavaca, Mor., Mexico*
[4] *Instituto de Investigaciones Metalúrgicas, Universidad Michoacana de San Nicolás de Hidalgo. Edificio "U", Ciudad Universitaria, 58066—Morelia, Michoacán, Mexico*

Correspondence should be addressed to J. G. Gonzalez-Rodriguez, ggonzalez@uaem.mx

Received 10 October 2011; Accepted 27 January 2012

Academic Editor: W. Ke

The effect of 2.5 at.% Cr, Ti, and Ag on the corrosion behavior of Fe40Al intermetallic alloy in KCl-$ZnCl_2$ (1 : 1 M) at 670°C has been evaluated by using electrochemical techniques. Techniques included potentiodynamic polarization curves, linear polarization resistance (LPR), and electrochemical impedance spectroscopy (EIS) measurements. Results have shown that additions of both Cr and Ti were beneficial to the alloy, since they decreased its corrosion rate, whereas additions of Ag was detrimental, since its additions increased the corrosion rate, although the alloy was passivated by adding Ag or Cr. The best corrosion performance was obtained with the addition of Cr, whereas the highest corrosion rate was obtained by adding Ag. This is explained in terms of the stability of the corrosion products formed film.

1. Introduction

Sodium and potassium impurities present in the form of chloride or sulfates are very corrosive constituents under certain combustion conditions such as waste incinerators and biomass-fired boilers [1, 2]. Early failure of the thermal components frequently occurs due to the complex reactions between the metallic materials and the hostile combustion environment. Incineration has become a viable technology for disposing of various types of wastes, including municipal, hospital, chemical, and hazardous. Problems with process equipment resulting from fireside corrosion have been frequently encountered in incinerators. The major problem is the complex nature of the feed (waste) as well as corrosive impurities which form low-melting point compounds with heavy and alkali metal chloride which prevents the formation of protective oxide scales and then causes an accelerated degradation of metallic elements [1]. In particular, under reducing conditions such as those typical of the operation of waste gasification plants or even under localized reducing conditions, which frequently arise in the case of incorrect operation of waste incineration systems, it is difficult to form protective oxide scales such as Cr_2O_3, SiO_2, and Al_2O_3 on the surface of structural materials. Thus, the corrosion attack can be further enhanced under reducing atmospheres in the presence of salt deposits [2].

The effect of individual KCl, NaCl, and their mixtures with heavy metal chlorides or sulfates on the corrosion behavior of a series of alloy systems has been studied in detail so far [3–9]. It is generally realized that Cr is not as effective element for corrosion resistance of Fe-base and Ni-based alloys due to chloride attack. In contrast, alumina- (Al_2O_3) forming alloys exhibit promising candidate materials considering the better high temperature resistance of alumina over chromia and their properties such as lower cost, low density, high strength, and good wear resistance [10–13].

In order to obtain more information on the corrosion mechanisms taking place, electrochemical techniques are more appropriated than gravimetric methods. Since a molten salt acts as an electrolyte, electrochemical techniques

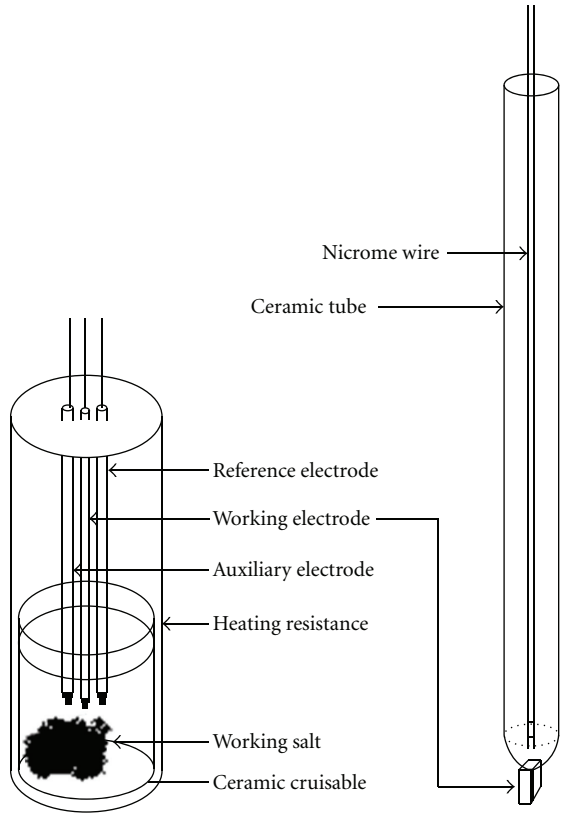

Figure 1: Schematic diagram showing the experimental setup.

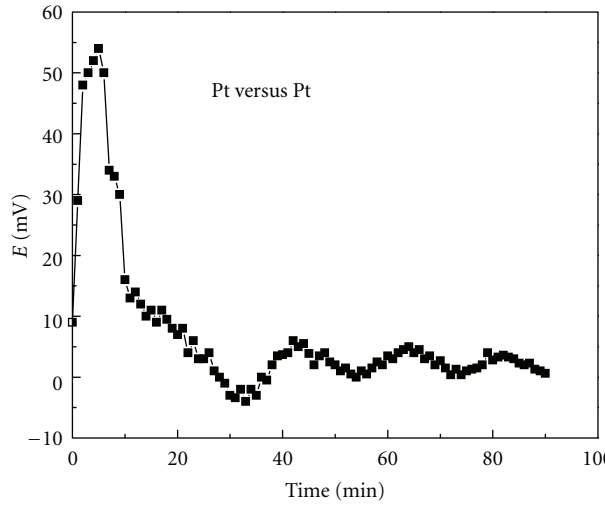

Figure 2: Potential fluctuations of a platinum reference electrode versus another platinum reference electrode.

such as potentiodynamic polarization curves and linear polarization resistance (LPR) measurements can be used just like Ducati et al. [14] showed in one of the earliest works on this topic. Zeng et al. used electrochemical impedance spectroscopy (EIS) studies for the corrosion of two-phase Cu-15Al alloy in the eutectic (Li, K)$_2$CO$_3$ at 650°C [15] and for Ni$_3$Al alloy in (Li, Na, K)$_2$SO$_4$ at 650°C [16]. They found that the complex plane of the electrochemical impedance suggested that the fast corrosion rate of these alloys was due to the formation of a nonprotective oxide, and that the corrosion process was controlled by the diffusion of oxidants. Shirvani et al. [17] used polarization curves to study the corrosion performance of the slurry Si-modified aluminide coating on the nickel base superalloy In-738LC exposed to Na_2SO_4—20 wt. % NaCl melt at 750°C. Zhu et al. [18] used Tafel extrapolation, linear polarization resistance, chronopotentiometry, and EIS to determine corrosion rates of iron and iron-based alloys in molten carbonate melts for both cathode and anode in molten carbonate fuel cell (MCFC) environments. Cuevas-Arteaga and coworkers [19–21] have successfully used electrochemical techniques to study the corrosion of materials used in sulfate+vanadate environments and obtained information about both the type and mechanisms of corrosion on these environments. This work deals with an electrochemical study of the effect of adding 2.5 at. % Cr, Ti, and Ag to a Fe40Al intermetallic alloy corroded in KCl-$ZnCl_2$ (1 : 1 M) at 670°C.

2. Experimental Procedure

Cast ingots of binary Fe-40 at. % Al and ternary Fe40Al-X (X = 2.5 at. % Cr, Ti or Ag) alloys were fabricated using a high-frequency vacuum induction furnace. Iron, Aluminum, Chromium of high purity (99.9%) were placed in an alumina crucible placed inside a graphite crucible in order to be induction melted under vacuum. The molten Fe-40Al, Fe40Al-X alloys were poured into a rectangular copper mould. The produced ingots were cut by a diamond wheel cutter in small rectangular parallelepiped pieces of surface area ranging from 1.5 to 2.5 cm^2. Electrochemical techniques included potentiodynamic polarization curves, linear polarization resistance (LPR), and electrochemical impedance spectroscopy (EIS) measurements. Details of the experimental setup for the electrochemical cell used in this work are given elsewhere [22]. The body of the cell was a 15 mL ceramic crucible. The most important elements were a reference and auxiliary electrodes, made of a 0.5 mm diameter platinum (Pt) wire inside a mullite tube and filled with commercial refractory, ceramic cement as shown in Figure 1. The amount of salt in each run was 0.5 g for an exposed area of 1.0 cm^2 under static conditions, without stirring the molten salt. The electrical contact was made by welding an 80 wt. % Cr—20 Ni, Nicrome wire to the specimen. The stability of the platinum reference electrode was measured by measuring its free corrosion potential versus another identical platinum reference electrode and the results are shown in Figure 2. We can see that during the first ten minutes the potential value shifted towards more active values for up to 55 mV more positive, but after this, the potential value dropped and reached a more or less stable value after approximately one hour or so. Polarization curves were obtained by polarizing the specimens from −500 to +1000 mV$_{Pt}$ with respect to the free corrosion potential value, E_{corr}, at a scanning rate of 1.0 mV/s. Corrosion current density values, I_{corr}, were calculated by using the Tafel

Table 1: Electrochemical parameters obtained from the polarization curves.

Alloy	E_{corr} (mV)	I_{corr} (mA/cm^2)	E_{pas} (mV)	I_{pas} (mA/cm^2)	E_{pit} (mV)
Fe-40Al	−330	0.3	—	—	—
Fe-40Al-2.5Cr	−975	0.8	−562	50	−337
Fe-40Al-2.5Ag	−98	9	87	7	360
Fe-40Al-2.5Ti	156	0.4	—	—	—

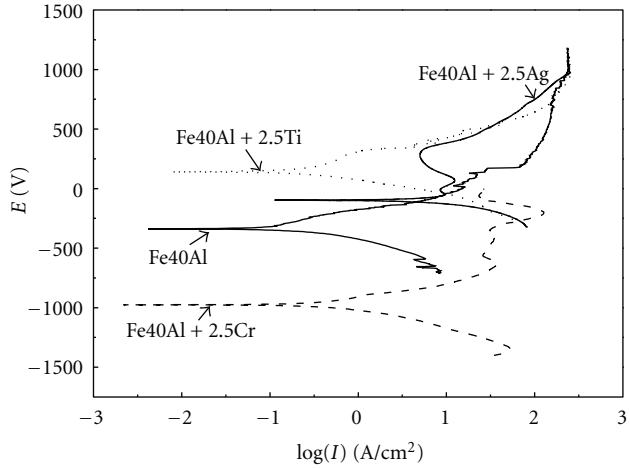

Figure 3: Polarization curves for Fe40Al alloyed with 2.5% Cr, Ti, and Ag in the KCl + $ZnCl_2$ mixture at 670°C.

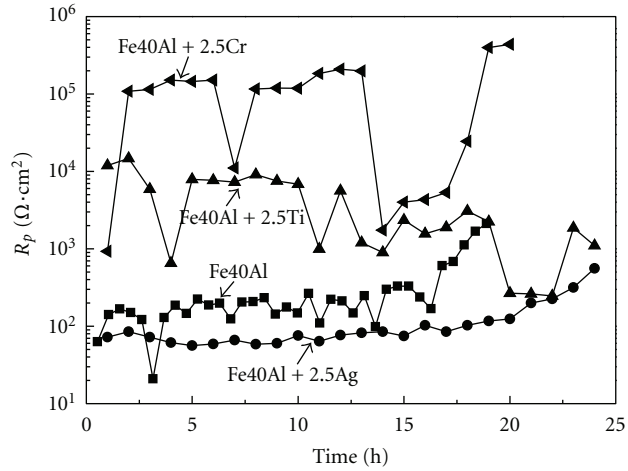

Figure 4: Change in the R_p value with time for Fe40Al alloyed with 2.5% Cr, Ti, and Ag in the KCl + $ZnCl_2$ mixture at 670°C.

extrapolation method, which is valid for the sweep rates used here according to [21] and taking an extrapolation zone of ± 250 mV around the E_{corr} value once it was stable. LPR measurements were carried out by polarizing the specimen from −10 to +10 mV with respect to E_{corr}, at a scanning rate of 1 mV/s every 20 minutes during 24 hours. EIS measurements were done in the frequency interval of 0.05 to 30000 Hz at the E_{corr} value by using a PC4-300 Gamry potentiostat. The amplitude of the input sine-wave voltage was 10 mV as recommended by previous works done on this topic [15, 16]. Working salt consisted of 500 mg/cm^2 of an eutectic mixture of KCl-$ZnCl_2$, 1 : 1 M, analytical grade for each test. The testing temperature was 670°C in static air condition. Prior the tests, the surfaces of specimens were prepared by the standard technique of grinding with SiC from 240 to 600 grit emery paper, washed with water, and degreased with acetone. Some specimens taken after the LPR measurements were mounted in bakelite and polished to analyze the corroded surface in a scanning electron microscope (SEM) with an accelerating voltage of 10 keV. Microchemical analysis was carried out with energy dispersive of X-ray analyzer (EDX) attached to the SEM.

3. Results and Discussion

Polarization curves for Fe40Al alloyed with 2.5% Cr, Ti, or Ag are shown in Figure 3. This figure shows that unalloyed Fe40Al intermetallic alloy shows an active behavior only, with an E_{corr} value close to −330 mV and a corrosion rate, expressed in terms of the I_{corr} value, close to 0.3 mA/cm^2. The anodic current density increases as the potential is made more anodic, but around 100 mV a kind of anodic limiting current density is reached, maybe because of the formation of a layer of corrosion products. With the addition of both Ti and Ag, the E_{corr} is made more active, reaching values of 156 and −98 mV, respectively. Similarly, the corrosion current density value increases in all cases, especially with the addition of 2.5Ag. Thus, the addition of Ag increases the corrosion current density value and shifted the E_{corr} value towards the active region, which shows that this element is detrimental for the base alloy. On the other hand, a passive region was found with Cr and Ag at a passivating potential value, E_{pas}, of −562 and 87 mV, respectively, reaching a much higher passive current density, I_{pas}, with Cr (around 35 mA/cm^2) than that reached with Ti (close to 5 mA/cm^2). Table 1 summarizes all these parameters, which shows the beneficial effect of both Cr and Ti.

The change in the linear polarization resistance value with time, R_p, for the different alloys in the KCl + $ZnCl_2$ mixture are shown in Figure 4. It can be seen that by alloying with either Ti or Cr the R_p value increases for up to 3 orders of magnitude in the case of Cr, and thus, a decrease in the corrosion rate. This can be due to the formation of an Al_2O_3 layer, probably reinforced with Cr_2O_3. In both cases, the R_p value shows a decrease, but after that it increases once again, indicating a disruption of the external protective

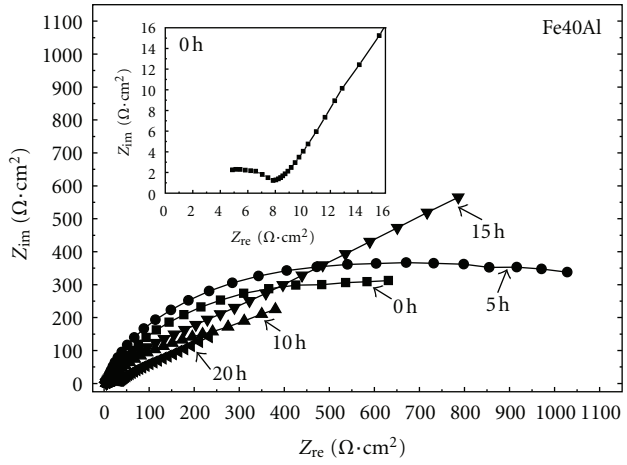

Figure 5: Nyquist diagrams for Fe40Al in the KCl + $ZnCl_2$ mixture at 670°C.

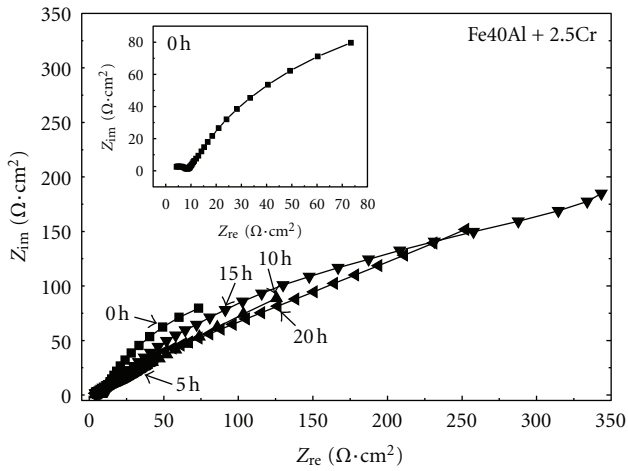

Figure 6: Nyquist diagrams for the Fe40Al + 2.5Cr alloy corroded in KCl + $ZnCl_2$ at 670°C.

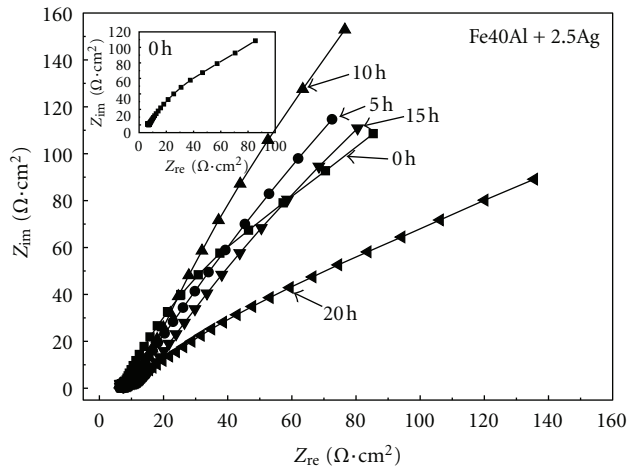

Figure 7: Nyquist diagrams for Fe40Al + 2.5Ag in the KCl + $ZnCl_2$ mixture at 670°C.

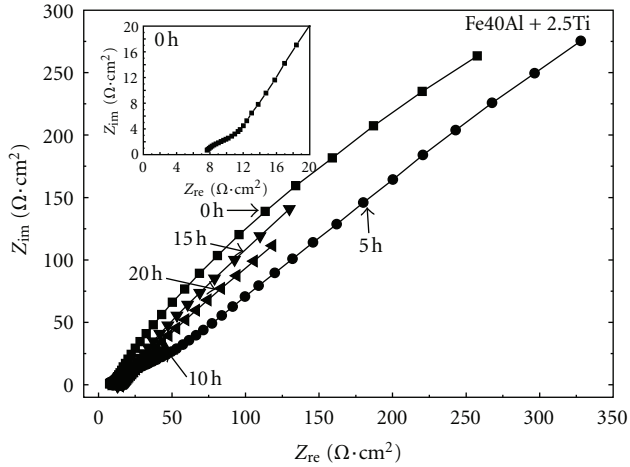

Figure 8: Nyquist diagrams for Fe40Al + 2.5Ti in the KCl + $ZnCl_2$ mixture at 670°C.

corrosion products layer, but a rapid re-establishment of it. Unlike this, the addition of 2.5Ag brings a decrease in the R_p value, and thus, an increase in the corrosion rate. The R_p value for unalloyed Fe40Al and Fe40Al + 2.5Ag intermetallic alloys shows a trend to increase as time increases, indicating a decrease in the corrosion rate and an increase in the protectiveness of the external layer, although this effect is marginal, not sufficient to reach the R_p values shown by the alloys containing either Cr or Ti. This means that the oxides formed in presence of Ag are more unstable as compared to those formed in presence of either Cr or Ti, leading to an increase in the corrosion rate for the alloy containing Ag.

Nyquist diagrams for unalloyed Fe40Al exposed to the KCl + $ZnCl_2$ mixture is shown in Figure 5, where it can be seen that for times shorter than 5 hours approximately, data describe a single capacitive-like semicircle, with its center in the real axis and its diameter increasing with time indicating that the corrosion process is under control by charge transfer from the metal to the electrolyte through the double electrochemical layer. For longer times than 5 hours or so, however, in addition to the high-frequency capacitive semicircle there is what seems an uncompleted low-frequency semicircle. The diameter of the low-frequency semicircle is much bigger than that for the high-frequency semicircle and it has a trend to decrease as time elapses. The emergence of a large capacitive loop at the low-frequency part may indicate the formation of a protective scale on the alloy surface.

For the alloy with addition of 2.5Cr, Figure 6, the data describes, at all exposure times, a semicircle at high and intermediate frequency values followed by a second semicircle at low-frequency values, with its diameter increasing with time. This time, the high-frequency semicircle diameter is lower than that for unalloyed Fe40Al base alloy, Figure 5. A similar behavior is observed for alloys with the addition of either Ag or Ti (Figures 7 and 8). However, the low-frequency

Table 2: Parameters used to simulate the EIS data for Fe-40Al-2.5Ag alloy.

Time (h)	R_s (Ohm cm^2)	R_{ct} (Ohm cm^2)	Y_{dl} (Ohm cm^{-2}s^{-n})	n_{dl}	Y_f (Ohm cm^{-2}s^{-n})	n_f	R_f (Ohm cm^2)
0	7.2	6.2	8.9×10^{-3}	0.80	9.2×10^{-3}	0.78	77.6
5	8.1	8.5	8.1×10^{-3}	0.77	9.9×10^{-3}	0.75	89.4
10	9.7	9.6	3.2×10^{-3}	0.71	3.8×10^{-3}	0.72	91.6
15	6.7	9.5	2.2×10^{-3}	0.51	7.5×10^{-3}	0.70	82.5
20	7.5	11.8	6.2×10^{-3}	0.32	7.4×10^{-3}	0.40	75.4

Table 3: Parameters used to simulate the EIS data for Fe- 40Al-2.5Ti alloy.

Time (h)	R_s (Ohm cm^2)	R_{ct} (Ohm cm^2)	Y_{dl} (Ohm cm^{-2}s^{-n})	n_{dl}	Y_f (Ohm cm^{-2}s^{-n})	n_f	R_f (Ohm cm^2)
0	7.2	10.7	1.3×10^{-3}	0.67	3.1×10^{-3}	0.59	9057
5	9.2	46.8	5.6×10^{-3}	0.43	2.5×10^{-3}	0.51	4736
10	9.4	11.8	3.9×10^{-2}	0.24	2.2×10^{-2}	0.59	8016
15	14	34.7	5.5×10^{-3}	0.66	7.4×10^{-3}	0.56	7784
20	12	13.5	5.7×10^{-3}	0.60	7.7×10^{-3}	0.54	2369

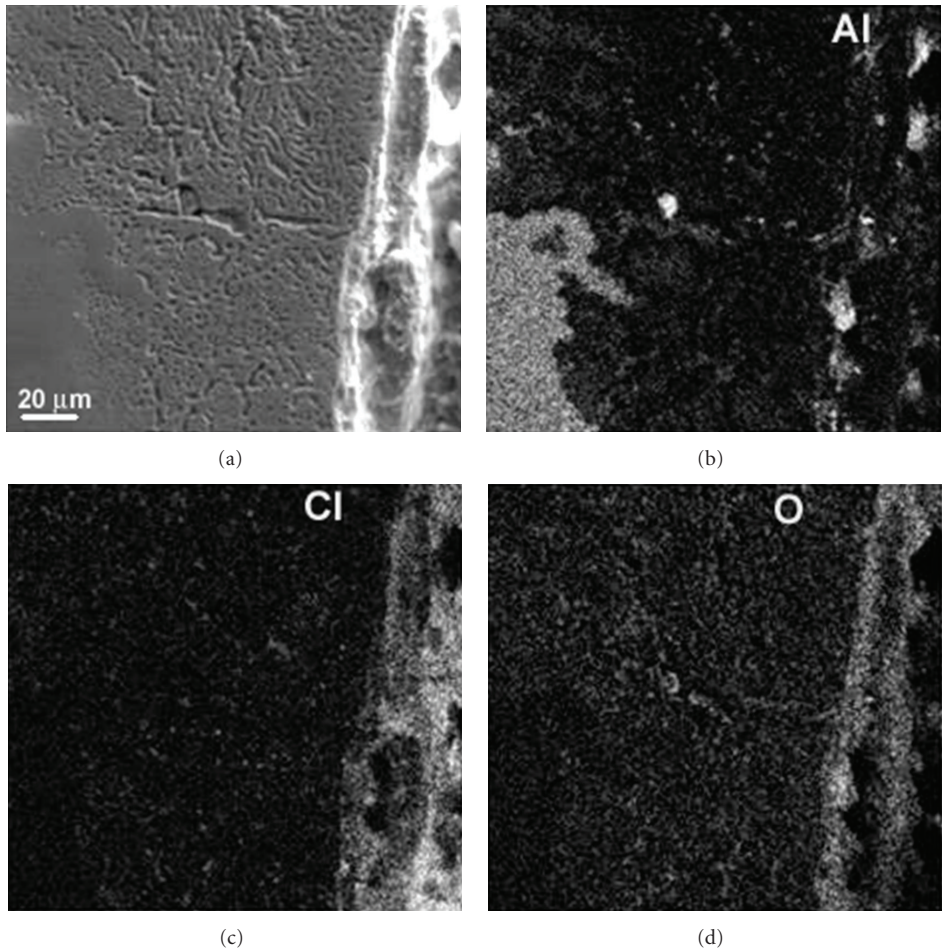

Figure 9: Microphotograph of Fe40Al corroded in the KCl + $ZnCl_2$ mixture at 670°C together with X-ray mappings of Al, Cl, and O.

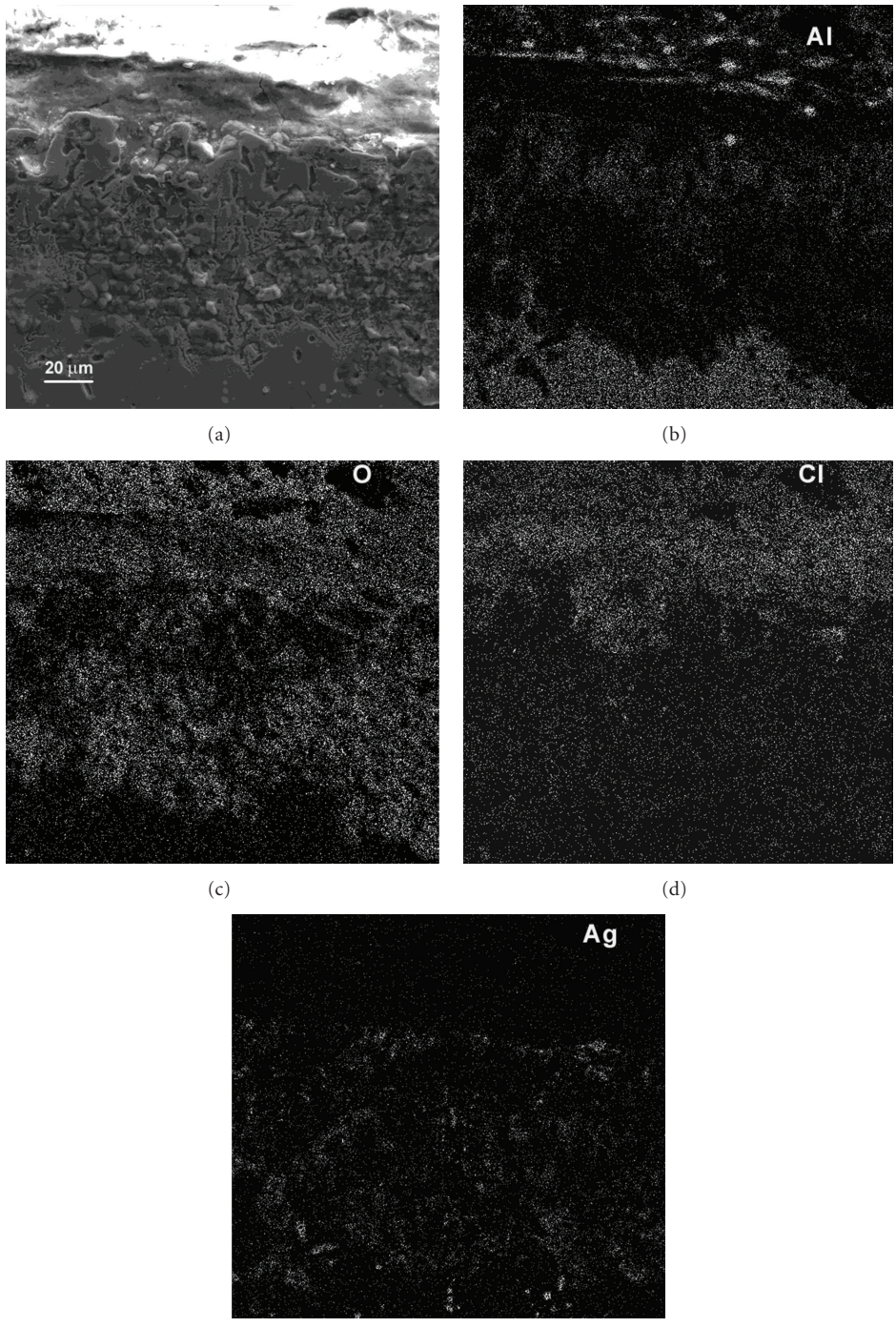

(a) (b) (c) (d) (e)

Figure 10: Microphotograph of Fe40Al + 2.5Ag corroded in the KCl + $ZnCl_2$ mixture at 670°C together with X-ray mappings of Al, Cl, O, and Ag.

semicircle diameter this time shows an erratic behavior, since sometimes it increases with time, and some other times it decreases. This explains why the addition of 2.5Ag increases the corrosion rate of the base alloy, since Nyquist diagrams show the formation of unstable oxides due to the disruption of the external layer formed by the corrosion products or to the dissolution of any protective oxide layer formed on top of the alloy, which is dissolved by the molten salt, Figures 3 and 4.

In order to have a better picture of this behavior, some micrographs of corroded specimens were examined in the scanning electronic microscope. Figure 9 shows a micrograph of corroded Fe40Al base alloy together with the corresponding X-ray mappings of Al, Cl, and O. The

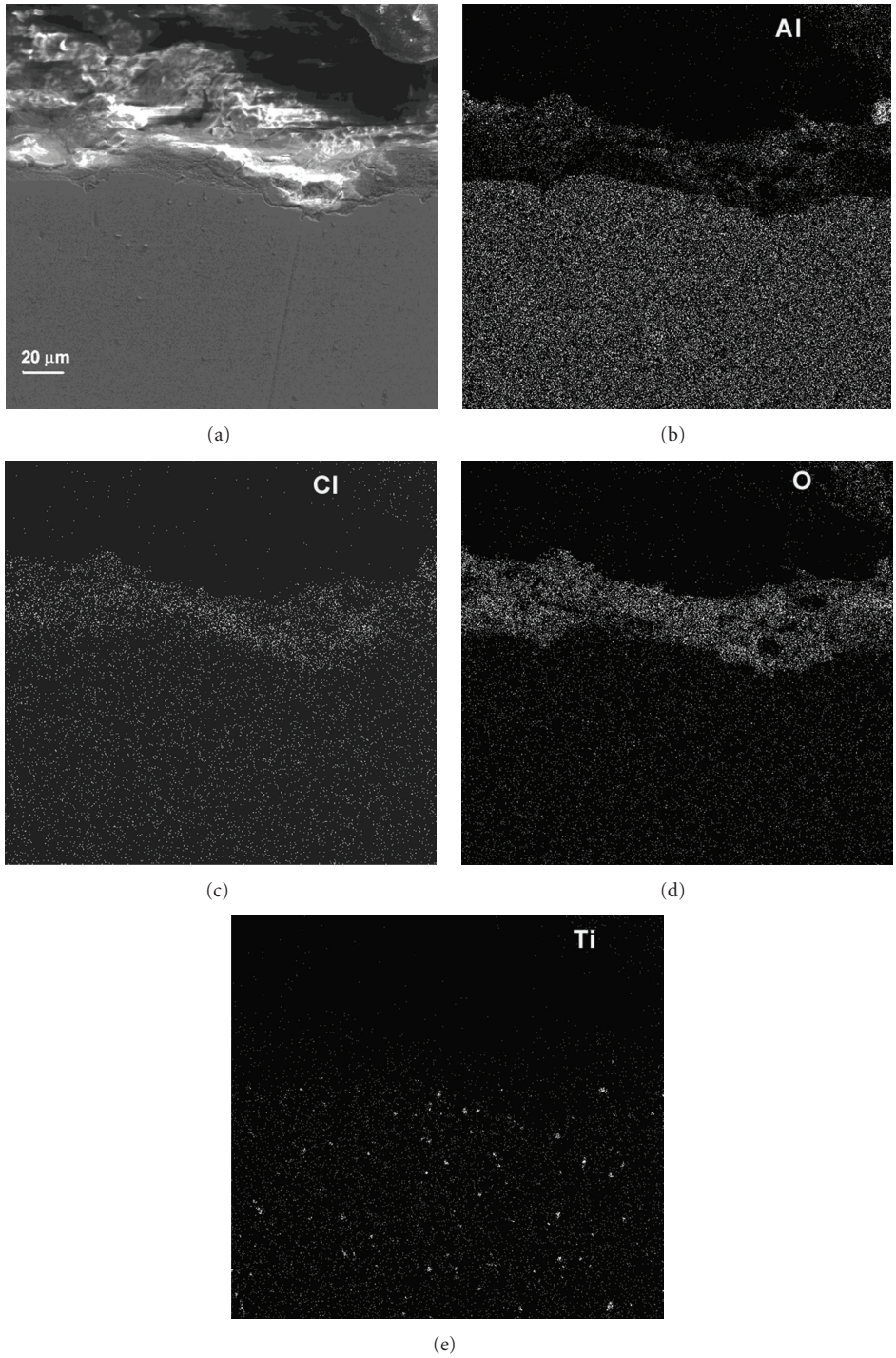

Figure 11: Microphotograph of Fe40Al + 2.5Ti corroded in the KCl + $ZnCl_2$ mixture at 670°C together with X-ray mappings of Al, Cl, O and Ti.

presence of O and Al on the external layer, although the Al-layer was not continuous, leads us to the assumption that there was some Al_2O_3 layer formed on top of the alloy. In addition to this, there is Cl present, which indicates that the molten salt has penetrated and dissolved the external, protective Al_2O_3 layer, leading to a continuous degradation of the alloy. Similar features were present the alloy with addition of Ag and Ti, Figures 10 and 11, respectively, where it can be seen the presence of an Al-containing oxide on the external surface, dissolved by chloride ions, although the oxide present in the Ag-containing alloy seems to be more porous than that present in the Ti-containing alloy. It can be seen that in the Ti-containing alloy the formed oxide is external and the presence of any Ti-containing oxide,

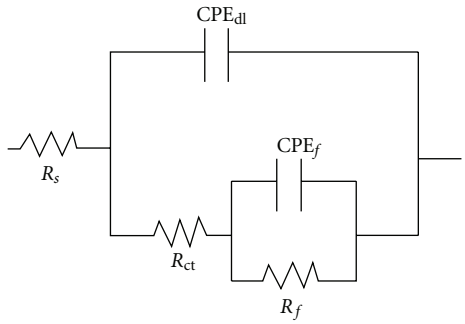

Figure 12: Electric circuit used to simulate the EIS data.

perhaps TiO_2 is in very negligible. On the other hand, on the Ag-containing alloy, it can be seen that Ag reacted more with O than Ti, the main corrosion product seems to be silver oxides with, such as AgO and Ag_2O and, maybe, some silver chloride, $AgCl_2$; maybe this is the reason why this alloy is less corrosion resistant than the one containing Ti.

EIS results can be represented by equivalent circuit shown on Figure 12, where R_s is the solution or electrolyte resistance, CPE_{dl} the double-layer capacitance, R_{ct} the charge transfer resistance, CPE_f the capacitance of any formed film on the surface, R_f its resistance. The impedance of a CPE is described by the expression [23]:

$$Z_{CPE} = Y^{-1}(j\omega)^{-n}, \quad (1)$$

where Y is the admittance, j is $\sqrt{-1}$ and ω is $2\pi f$ and f the used frequency. As an example of this, Tables 2 and 3 give the parameters used to simulate the EIS data for Fe40Al with 2.5Ag and 2.5Ti, respectively. It can be seen that, generally speaking, the R_{ct} values for both alloys are smaller than the corrosion products resistance, R_f, indicating that the corrosion resistance of both alloys is given by this film. However, the R_f value for the Ti-containing alloy shows an erratic behavior as time elapses, that is, the film thickness decreases and increases, indicating that the film is constantly detached from the alloy surface. In addition to this, the values of n_{dl} and n_f deviate from 1, indicating a strong dispersion effect which is common in molten salt corrosion [24]. Moreover, their values at the later stage were smaller than those at the initial stage, which may be related to the partial loss of the molten salt due to evaporation or to the roughness of the surface oxide layer.

4. Conclusions

A study of the effect of 2.5 at. % Cr, Ag, and Ti on the corrosion behavior of Fe40Al in molten KCl-$ZnCl_2$ (1 : 1 M) at 670°C has been carried out by using electrochemical techniques. Polarization curves have shown that by adding either Cr or Ag the alloy was passivated, although the passive current density was higher with the later. Addition of either Cr or Ti were beneficial, since the lowest corrosion rate was obtained by their addition, whereas the highest corrosion rate, even lower than that obtained with the unalloyed Fe40Al base alloy, was obtained by adding 2.5Ag, being the addition of this element detrimental for the alloy. EIS data showed that the corrosion rate was controlled by the formation of an external corrosion products external film, which was dissolved by the Cl-containing molten salt. The stability of this external film provides the corrosion resistance of the alloy.

References

[1] H. J. Grabke, E. Reese, and M. Spiegel, "The effects of chlorides, hydrogen chloride, and sulfur dioxide in the oxidation of steels below deposits," *Corrosion Science*, vol. 37, no. 7, pp. 1023–1043, 1995.

[2] W. M. Lu, T. J. Pan, K. Zhang, and Y. Niu, "Accelerated corrosion of five commercial steels under a $ZnCl_2$–KCl deposit in a reducing environment typical of waste gasification at 673–773 K," *Corrosion Science*, vol. 50, no. 7, pp. 1900–1906, 2008.

[3] Y. S. Li, M. Spiegel, and S. Shimada, "Corrosion behaviour of various model alloys with NaCl–KCl coating," *Materials Chemistry and Physics*, vol. 93, no. 1, pp. 217–223, 2005.

[4] Y. Shibata, "Cyclic oxidation behavior of Ni3Al–0.1B base alloys containing a Ti, Zr, or Hf addition," *Oxidation of Metals*, vol. 26, no. 3, pp. 201–207, 1986.

[5] N. Hiramatsu, Y. Uematsu, T. Tanaka, and M. Kinugasa, "Effects of alloying elements on NaCl-induced hot corrosion of stainless steels," *Materials Science and Engineering A*, vol. 120, no. 11, pp. 319–328, 1989.

[6] Y. S. Li, M. Sanchez-Pasten, and M. Spiegel, "Fundamental studies on alkali chloride induced corrosion during combustion of biomass," *Materials Science Forum*, vol. 461, no. 3, pp. 1047–1052, 2004.

[7] F. Wang, Y. Shu, and W. P. Pan, "High-temperature corrosion of A210–C carbon steel in simulated coal-combustion atmospheres," *Oxidation of Metals*, vol. 59, no. 2, pp. 201–208, 2003.

[8] C. J. Wang and Y. C. Chang, "NaCl-induced hot corrosion of Fe–Mn–Al–C alloys," *Materials Chemistry and Physics*, vol. 76, no. 2, pp. 151–157, 2002.

[9] Y. S. Li, Y. Niu, and W. T. Wu, "Accelerated corrosion of pure Fe, Ni, Cr and several Fe-based alloys induced by $ZnCl_2$–KCl at 450°C in oxidizing environment," *Materials Science and Engineering A*, vol. 345, no. 3, pp. 964–970, 2003.

[10] F. H. Stott and G. C. Wood, "Internal oxidation," *Materials Science and Technology*, vol. 4, no. 12, pp. 1072–1078, 1988.

[11] G. Han and W. D. Cho, "High-temperature corrosion of Fe_3Al in 1% Cl_2Ar," *Oxidation of Metals*, vol. 58, no. 3-4, pp. 391–413, 2002.

[12] F. Lang and Z. Yu, "Corrosion behavior of Fe–40Al sheet in N_2–11.2O_2–7.5CO_2atmospheres with various SO_2 contents at 1273 K," *Intermetallics*, vol. 11, no. 2, pp. 135–141, 2003.

[13] Y. Kawahara, "High temperature corrosion mechanisms and effect of alloying elements for materials used in waste incineration environment," *Corrosion Science*, vol. 44, no. 2, pp. 223–232, 2002.

[14] U. Ducati, G. L. Coccia, and G. Caironi, "Electrochemical evaluation of hot corrosion resistance of metallic materials," *Materials Chemistry and Physics*, vol. 8, no. 2, pp. 135–145, 1983.

[15] C. L. Zeng, P. Y. Guo, and W. T. Wu, "Electrochemical impedance spectra for the corrosion of two-phase Cu–15Al alloy in eutectic (Li, K)$_2CO_3$ at 650°C in air," *Electrochimica Acta*, vol. 49, no. 9, pp. 1445–1450, 2004.

[16] C. L. Zeng, W. Wang, and W. T. Wu, "Electrochemical impedance models for molten salt corrosion," *Corrosion Science*, vol. 43, no. 4, pp. 787–801, 2001.

[17] K. Shirvani, M. Saremi, A. Nishikata, and T. Tsuru, "Electrochemical study on hot corrosion of Si-modified aluminide coated In–738LC in Na_2SO_4–20 wt.% NaCl melt at 750°C," *Corrosion Science*, vol. 45, no. 5, pp. 1011–1021, 2003.

[18] B. Zhu, G. Lindbergh, and D. Simonsson, "Electrochemical impedance studies of the initial-stage corrosion of 310 S stainless steel beneath thin film of molten $(0.62Li, 0.38K)_2CO_3$ at 650°C," *Corrosion Science*, vol. 41, no. 9, pp. 1497–1513, 1999.

[19] C. Cuevas-Arteaga, J. Uruchurtu-Chavarín, J. Porcayo-Calderon, G. Izquierdo-Montalvo, and J. Gonzalez, "Study of molten salt corrosion of HK–40 m alloy applying linear polarization resistance. And conventional weight loss techniques," *Corrosion Science*, vol. 46, no. 11, pp. 2663–2679, 2004.

[20] C. Cuevas-Arteaga, J. Uruchurtu-Chavarín, J. G. González, G. Izquierdo-Montalvo, J. Porcayo-Calderón, and U. Cano, "Corrosion evaluation of Alloy 800 in sulfate/vanadate molten salts," *Corrosion*, vol. 60, no. 4, pp. 520–527, 2004.

[21] C. Cuevas-Arteaga, "Corrosion study of HK–40 m alloy exposed to molten sulfate/vanadate mixtures using the electrochemical noise technique," *Corrosion Science*, vol. 50, no. 3, pp. 650–663, 2008.

[22] J. G. Gonzalez-Rodriguez, O. L. Arenas, J. Porcayo-Calderon, V. M. Salinas-Bravo, M. Casales, and A. Martinez-Villafañe, "An electrochemical study of the effect of B on the corrosion of atomized Fe40Al intermetallics in molten Na_2SO_4," *High Temperature Materials and Processes*, vol. 25, no. 2, pp. 293–301, 2006.

[23] J. R. MacDonald, "Equivalent circuits for the binary electrolyte in the Warburg region," *Journal of Electroanalytical Chemistry*, vol. 223, no. 9, pp. 182–189, 1987.

[24] C. S. Ni, L. Y. Lu, C. L. Zeng, and Y. Niu, "Electrochemical impedance studies of the initial-stage corrosion of 310 S stainless steel beneath thin film of molten $(0.62Li, 0.38K)_2CO_3$ at 650°C," *Corrosion Science*, vol. 53, pp. 1018–1024, 2011.